Development and Expansion of a Medical System Using Non-contact Energy Transmission Technology via Fusion between the Living Body and Electromagnetic Field

Hidetoshi Matsuki[1,2)]

Professor
1) Graduate School of Biomedical Engineering
2) Graduate School of Engineering
E-mail: matsuki@ecei.tohoku.ac.jp

1. Abstract

Emphasis has recently been placed on the linkage between medicine and engineering, with numerous achievements been made such as therapeutic diagnostic devices and artificial organs. In the field of electrical engineering, supply of power to medical devices is an extremely important issue. Realization of energy efficiency and non-contact communication is essential to the future development of medical devices and welfare equipment. Non-contact energy transmission that sends energy without using a cable becomes the key to developing next-generation medical devices and welfare equipment.

If energy —especially electricity— is to be transmitted in a non-contact manner, use of a magnetic field that can attain high energy density and efficiency is best suited for this purpose. Even under a special environment like a living body, moreover, magnetic fields are affected very little. By using a frequency band that is known to have little impact on the living body, it is possible to transmit magnetic energy to the deep areas. By actively applying this magnetic field to biological devices, we have been realizing the transmission of non-contact energy. This paper describes the current status of the development and spread of hyperthermia, functional electrical stimulations, and the real-time dose measurement system.

2. Hyperthermia

Hyperthermia refers to thermotherapy performed for cancer, which is the leading cause of death among the Japanese people. Cancer is generally treated by surgery, chemotherapy, and radiation. Hyperthermia is drawing attention as a new treatment method that follows these conventional therapies.

As the name implies, hyperthermia is a method of necrotizing cancer tissues using heat. Cancer tissues have insufficient vascular formation, so the cooling effects by the blood flow are low. This makes them more susceptible to temperatures than normal tissues. Whereas the survival rate of normal tissues drops at 44°C, that of cancer tissues is known to drop at 42.5°C.

There are several types of hyperthermia. Our research uses the soft-heating method.[1,2]. In this method, a long, thin, small heater element is embedded inside the body and heated, using a high-frequency magnetic field. Figure 2-1 shows the heater element. It is comprised of a thermosensitive magnetic body having a relatively low Curie temperature, and a metallic ring. Hysteresis loss and short-circuit current loss are the sources of heat generation. Each can realize greater temperature elevations than when heated

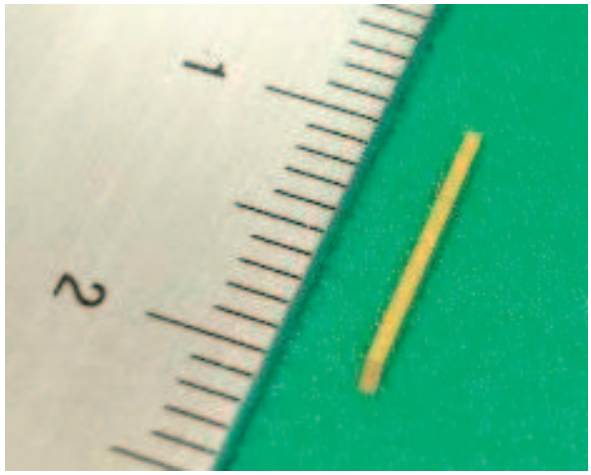

Fig. 2-1. Heat element

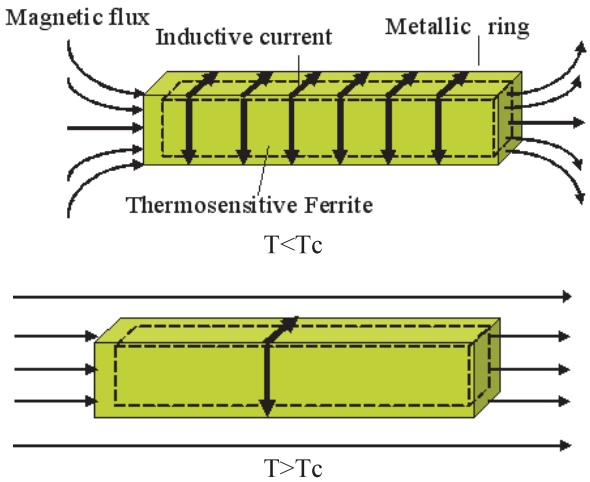

Fig. 2-2. Principle of heating

individually, making it possible to obtain high heat generation under low excitation conditions. Other types of hyperthermia require adjustment of the heat generation volume, and most warming methods require measurement of temperature of the affected areas. A major advantage of this method is that no measurement of temperature of the affected areas is required. Heating elements generate heat in a constant wall temperature-type fashion by Curie temperature (hereinafter referred to as "T_C"). The principle of heat generation is shown in Fig. 2-2. First, before the temperature reaches T_C, heat is generated by the thermosensitive magnetic body's hysteresis loss and the metallic ring's short-circuit current loss. Once the temperature exceeds T_C, however, the rate of effective magnetic permeability drops sharply, and the magnetic flux's concentrated effects become lost. Heat generation and elevation of temperature are suppressed as a result. Because of this, since the heating element itself possesses temperature self-control properties, of not elevating above the Curie temperature that has been set, it is possible to warm and necrotize the affected area only in the necessary sections. The sites never get overheated, either. In other words, safe treatment becomes possible. This method can be applied to an extremely large number of sites, since it can warm any part of the body, as long as it is a site where the elements can be embedded, and is within the scope where the excited magnetic field from the coil can reach.

2.1. Excitation coil aimed at multi-directional magnetic excitation

Heating elements generate heat the most efficiently when placed in line with the direction of the magnetic field, and the least efficiently when they are tilted at a 90-degree angle from the magnetic field. Therefore, depending on the shape of the human body, the site of treatment, or the placement of the elements, there may be cases when sufficient warming effects cannot be achieved with conventional solenoid or spiral coils. Thus, we need a coil that allows multi-directional excitation that can provide warming regardless of the position or direction of the elements that had been installed. To make this possible, we conducted simulations by taking note of the direction of the magnetic field, performed additional warming experiments by actually creating such coils, and verified the results. The kinds of cancer targeted in these experiments were superficial types such as skin and breast cancers.

In the case of single solenoid coils and spiral coils, the direction of the magnetic field mainly used for excitation is constant. We therefore studied causing excitation in a multiple direction, using two coils. Figure 2-3 shows one of the models that can cause such multi-directional excitations. This model is designed so that the magnetic field generated in the middle of the two solenoid coils meets orthogonally (hereinafter referred to as the "orthogonal type"). The excited electrical current and the frequency are the same. If the phase difference of the excited electrical currents of the two coils is set at 90 degrees, a rotational magnetic field is formed at the center point of the coil, as shown in Fig. 2-4. We can therefore see that the coil has been excited multi-directionally. For Fig. 2-4, the magnetic flux density generated from Coil 1 was set as B_X, and that generated from Coil 2, as B_Y, and the amounts were calculated by synthesizing hourly vectors, using the following formula:

$$B_X = B_0 \sin\omega \quad (1)$$

$$B_Y = B_0 \sin(\omega t+\pi/2)=B_0 \cos\omega t \quad (2)$$

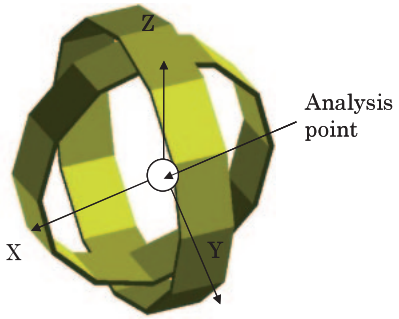

Fig. 2-3. Simulation model of orthogonal type

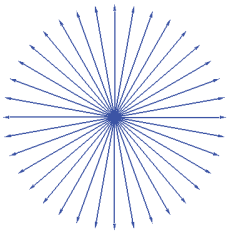

Fig. 2-4. Result of orthogonal type's simulation (Same frequency)

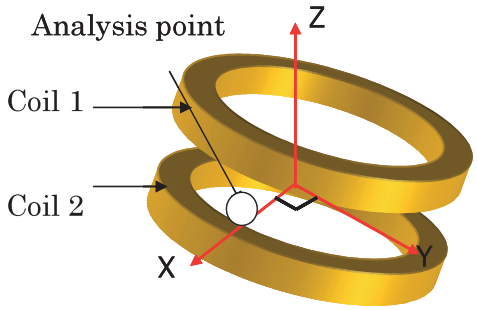

Fig. 2-5. Simulation model of cusp type

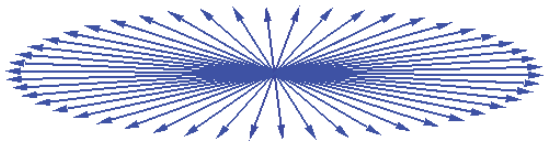

Fig. 2-6. Result of cusp type's simulation (Same frequency)

However, it is difficult to actually install such orthogonal-type models in the human body. We therefore conducted a simulation on a model that placed two (same-specification) solenoid coils in parallel, as shown in Fig. 2-5. In the present study, a coil that forms a cusp magnetic field that seals in plasma can be anticipated with this model, so we named it “cusp type.” This model is intended to be used by having it pass through the affected areas such as skin cancer that has developed on the arms and legs, etc., as well as breast cancer. The site where multi-directional magnetic field is generated is close to the coil’s inner circumference on the center plane between the coils, so we took an analysis point here. Figure 2-6 shows the results of Fig. 2-5’s analysis point. We can see that a multi-directional magnetic field can be obtained at the edge of the center plane between the coils, or, in other words, near the inner circumference of the coil.

Using two coils is effective for multi-directional excitations. However, when 2 coils are excited using the same frequency, there is a risk that electromagnetic coupling may cause the electric current to flow backwards to the other side and break the power source. This makes the design extremely difficult. We therefore considered activating two coils under different frequencies. We found that power source breakage could be prevented if we used a permeation filter that had been set differently according to frequency. We subsequently studied the direction of the magnetic field as well.

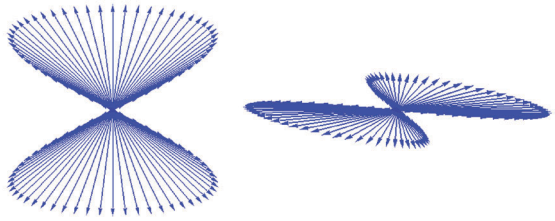

(a) Orthogonal type (b) Cusp type

Fig. 2-7. Result of simulation at analysis point (Combination of 100 kHz and 200 kHz)

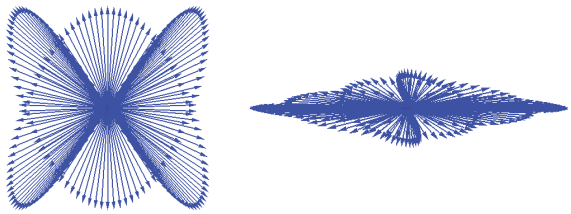

(a) Orthogonal type (b) Cusp type

Fig. 2-8. Result of simulation at analysis point (Combination of 100 kHz and 150 kHz)

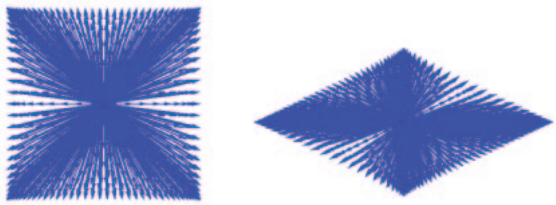

(a) Orthogonal type (b) Cusp type

Fig. 2-9. Result of simulation at analysis point (Combination of 130 kHz and 200 kHz)

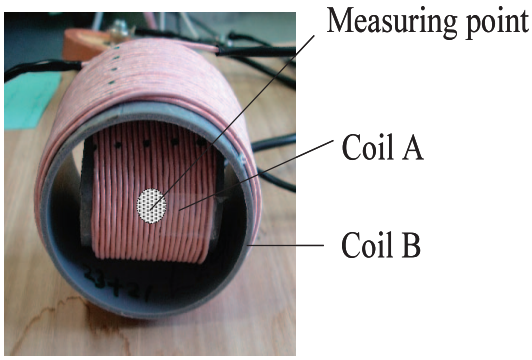

Fig. 2-10. Coil model of orthogonal type

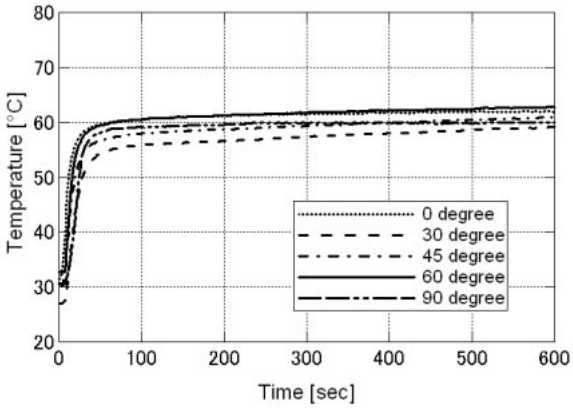

Fig. 2-11. Temperature characteristic of the surface of the element excited by the orthogonal model coil (Frequency 133 kHz and 193 kHz)

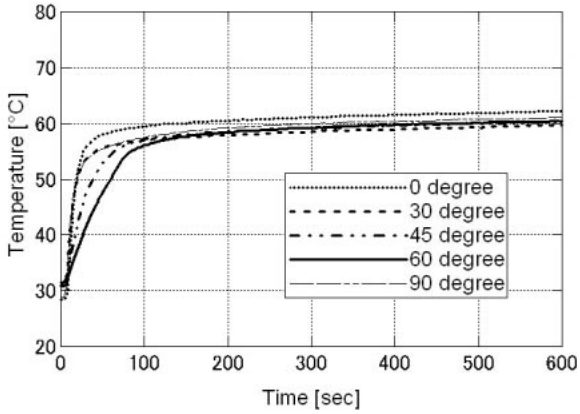

Fig. 2-12. Temperature characteristic of the surface of the element excited by the orthogonal model coil (Frequency 133 kHz)

Using the same procedure as when the same frequency was adopted, we conducted a simulation with each coil being activated with different frequencies. The analysis points were the same as those shown in Figs. 2-3 and 2-5. As examples of the simulation results, Fig. 2-7 shows the findings when frequencies 100 kHz and 200 kHz were used; Fig. 2-8 shows the findings when frequencies 100 kHz and 150 kHz were used; and Fig. 2-9 shows the findings when frequencies 130 kHz and 200 kHz were used, for both the orthogonal type and the cusp type. From these results, we can confirm that, although a range existed where no excitation could be generated depending on the combination of frequencies, such as the combination of 100 kHz and 200 kHz shown in Fig. 2-7, multi-directional excitation is possible at analysis points, more-so than a single coil.

Based on the simulation results described above, we conducted actual warming experiments, using an orthogonal model whose electromagnetic coupling is extremely small. We used solenoid coils with a diameter of 55 mm (Coil A) and 80 mm (Coil B), arranged them as shown in Fig. 2-10, and conducted the experiment. The frequency was 133 kHz for Coil A and 193 kHz for Coil B because we obtained findings, from Fig. 2-9, that multi-directional excitation was possible. We also set the electrical current value so that each coil could obtain a magnetic flux density of 3 mT at the measurement points (the central point of the two coils). The heating element whose Curie temperature was 70°C was wrapped in insulating material, and the element's surface temperature was measured for 10 minutes, using an optical fiber thermometer. To confirm multi-directional excitation at the measurement points, we conducted further experiments by varying the angle of the heating element. The results are shown in Fig. 2-11. For comparison, Fig. 2-12 shows the results of an experiment conducted under the same conditions with the same frequency but with the electrical current phase difference of 90 degrees, and Fig. 2-13 shows those using a single solenoid coil with a frequency of 200 kHz and a magnetic flux density of 0.5 mT. We can confirm, from these graphs that, even if different frequencies were adopted, the heating element could generate heat as favorably as when the same frequencies were used, and that multi-directional excitation was possible, more than when a single coil was used.

2.2. Summary of hyperthermia

We simulated two types of coil models that can cause multi-directional excitations (orthogonal and cusp types), and conducted experiments using the orthogonal type. Our results confirmed that, by using two coils, it was possible to warm the heating element installed in diverse directions. It can be said, therefore, that activating two coils under different frequencies can avoid the power source problem and is more effective for multi-directional excitations than a single coil.

In the future, there is a need to confirm the warming process, using cusp and other models that have larger coupling coefficients. This should enable diverse coil placements and combinations under different forms and shapes. It also becomes possible to create coil models that can be actually installed in the affected area and are optimally suited to the affected sites, helping the treatment process.

3. Functional Electrical Stimulation

When people are suffered Spinal Code Injury (SCI) by several accidents, the order signals from their brain aren't transmitted to their muscles and they become paralyzed. In some cases, however, their muscles can be constricted by applying electrical stimulation because their muscles keep excitability. And controlling pattern of these electrical stimulation is enable to rehabilitate their move functions. This therapy for paralyzed patients is Functional Electrical Stimulation (FES).

FES is classified according to the way to applying electrical stimulation. In the way with surface electrodes, mounting electrodes and stimulating are easier and surgical treatment is not necessary. But only a small part of a muscle can be stimulated, causing a rapid development of muscle fatigue. Furthermore, the reproducibility of muscle force is insufficient due to changes in the muscle geometry during contraction. On the other hand, the percutaneous electrode can stimulate several muscles with low energy and does not depend on the geometry of the muscle [3]. However, there are some problems due to the breaking of wire which is set in the body and infection disease on the penetrate points.

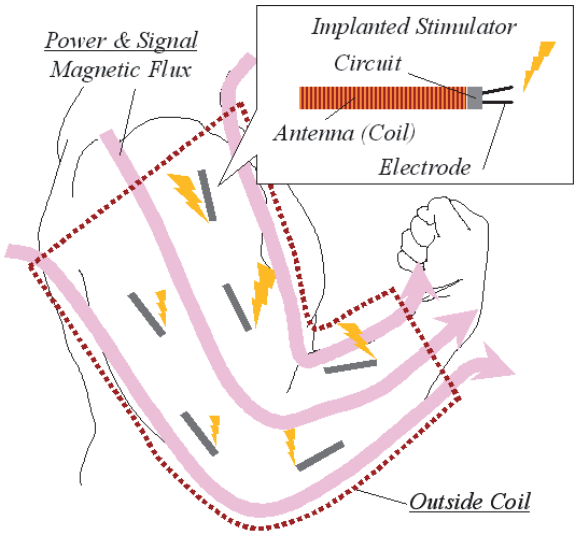

Fig. 3-1. The image of Direct Feeding Method (DFM). In the DFM, small implanted stimulators give stimuli for muscles applying driving and stimulus energy and controlling information with magnetic coupling.

The implanted Direct Feeding Method (DFM) solves these problems [4] . In this technique, small stimulators are implanted near the target points, and electrical stimuli are applied to them (Fig. 3-1). Implanted stimulators have an antenna, which is constructed of coils and capacitors. Driving and stimulus energy and stimulus pattern signals are applied by a mounted coil using magnetic coupling. This allows high-precision stimulation without percutaneous points and long wires.

In the implanted DFM, feedback information from the implanted stimulating system is necessary to confirm the operation of the system and safe usage, or to enable the DFM of FES to rehabilitate more complex motor functions. However, we have not developed an implanted unit that has such a function. In this study, we invented the duplex communicable implanted antenna. We report the advanced antenna that we proposed and the communication results to verify the ability of the antenna.

3.1. Principle of antenna

We proposed the Magnetic Connective Dual Resonance (MCDR) antenna as an implanted duplex communication antenna. The composition of MCDR antenna is shown in Fig. 3-2. This antenna has two resonance circuits connected magnetically each other in order to function as duplex communication antenna.

When the MCDR antenna sends the signal, the current which value is proportional to the value of signal voltage flows in Lp, and the magnetic flux is generated from Lp. The signal voltage is not so large that the value of magnetic flux from Lp is not enough to send signal. And then, the magnetic flux from Lp enters into the resonant circuit Rs, the current flowing in Rs is resonated and is enlarged because the circuit Rs is serial resonate circuit for the induced current. Meanwhile, at the receiving, the capacitor Cp is resonated with the circuit Rp and the large signal voltage is applied to Cp.

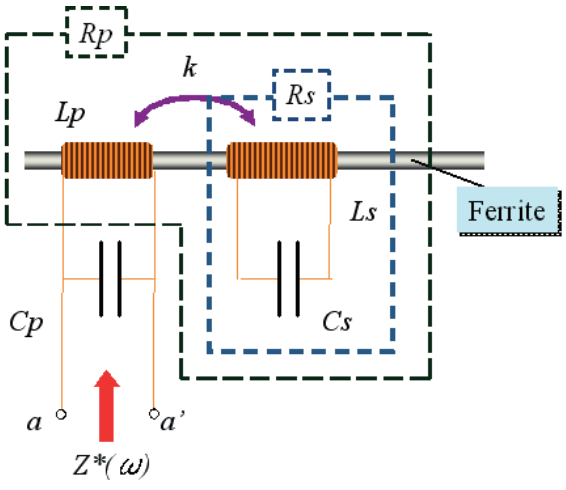

Fig. 3-2. Composition of MCDR Antenna

3.2. Impedance analysis

The impedance at the view points of a-a' is expressed as expression (3-1).

$$Z^*(\omega) = j\omega Lp \frac{1-\omega^2 CsLs(1-k^2)}{1-(CpLp+CsLs)\omega^2+CpLpCsLs(1-k^2)\omega^4} \quad (3\text{-}1)$$

$$f_{io} = \frac{1}{2\pi\sqrt{LsCs(1-k^2)}} \quad (3\text{-}2)$$

$$f_{oi} = \frac{1}{2\pi}\sqrt{\frac{CpLp+CsLs \pm \sqrt{(CpLp-CsLs)^2-4CpLpCsLsk^2}}{CpLpCsLs(1-k^2)}} \quad (3\text{-}3)$$

Where, the resistances of coils have been no concerned. It is well known that the antenna can transmit signals or receive signals at the frequency at which the impedance becomes zero or infinity. Therefore the expression (3-1) gives transmitting frequency fio and receiving frequency foi as following expressions.

Because these frequencies are real number, the MCDR antenna is able to become sending and receiving mode. In addition, the values of capacitances are following formulas.

3.3. Optimal coupling coefficient

If the coupling coefficient between Lp and Ls is too small, the MCDR antenna can not send the signal. The larger, on the other hand, the larger magnetic energy is transmitted from Lp to Ls, but too strong coupling enlarges the mutual inductance between Lp and Ls, and slows down the performance. So we analyzed the relation between the coupling coefficient and the received voltage.

We analyzed the voltage at Rload altering coupling coefficient between Lp and Ls. Figure 3-3 shows the simulated circuit and circuit parameters are described in Table. 3-1. The resonant frequencies are aimed at below; fio = 2.0MHz and foi = 1.6MHz. The value of Inductances and resistances are determined by experimental rule. Cp and Cs are depended on the expression (3-4) and (3-5).

$$Cs = \frac{1}{(2\pi f_{io})^2 Ls(1-k^2)} \quad (3\text{-}4)$$

$$Cp = \frac{1}{(2\pi f_{oi})^2 Lp} \frac{1-(2\pi f_{oi})^2 LsCs}{1-(2\pi f_{oi})^2 LsCs(1-k^2)} \quad (3\text{-}5)$$

The result is shown in Fig. 3-4. Communication is the easiest when k = 0.45 at the sending from the implant and k = 0.20 at the receiving at the implant. Although both sending and receiving function is higher performance at about 0.33, we aimed at 0.45 because of lower energy of implant devices than the device which is outside the body.

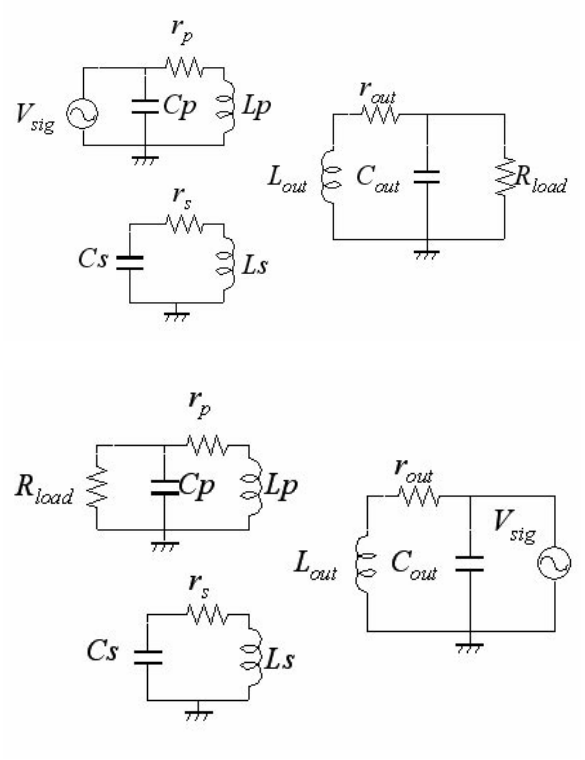

Fig. 3-3. Simulated Circuit for optimize coupling coefficient between Lp and Ls. The left circuits signify the implanted antenna (MCDR), and the other circuit is the mounted antenna. (a) is the circuit diagram of transmission information from inside the body to outside (Sending), and (b) is the other (Receiving).

Table 3-1. Parameters in the Simulated Circuits

k	$k\ (Lp - L_{out})$	
	$k\ (Ls - L_{out})$	0.001
L	Lp [μH]	20
	Ls [μH]	30
	L_{out} [μH]	30
r	r_p [Ω]	5
	r_s [Ω]	10
	$Rout$ [Ω]	0.5
R_{load} [MΩ]		1

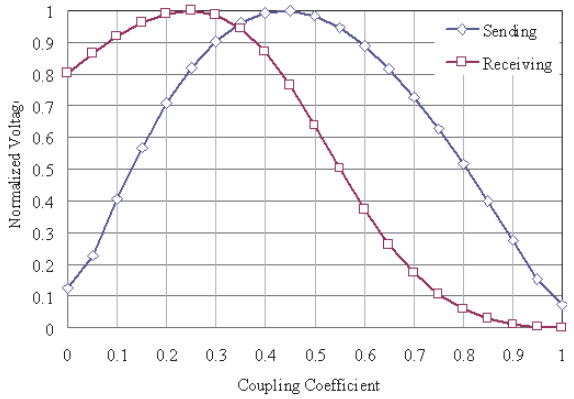

Fig. 3-4. Received voltage at the Rload vs coupling coefficient between Lp and Ls.

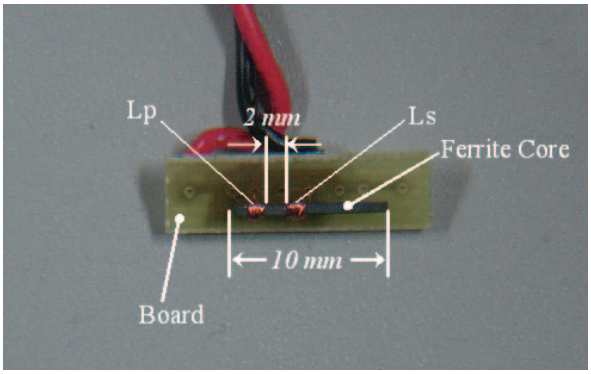

Fig. 3-5. Image of the MCDR antenna. The ferrite is 0.7 by 0.7 by 10 mm, and capacitors Cp, Cs are mounted back of the board.

Table 3-2. Specific of MCDR Antenna

k		0.465
r*	r_p [Ω]	4.63
	r_s [Ω]	8.34
L*	Lp [μH]	17.89
	Ls [μH]	26.22
C	Cp [pF]	280
	Cs [pF]	309

* at 2 MHz

3.4. Experimental

We made the MCDR antenna depending on above, and show this in Fig. 3-5. Capacitances are mounted back of the board. The ferrite core is N-120L and its size is 0.7 by 0.7 by 10 mm. The distance between Lp and Ls is 2 mm and coupling coefficient is 0.465. The detail of this antenna is described in Table 2.

The frequency characteristics of the impedance of this MCDR antenna and of the theoretical impedance are shown in Fig. 3-6. Although the actual characteristics denotes the same tendency of the theoretical, the resonant frequency at the higher local maximum frequency is out of alignment. This is why the magnetic interference between Lp and Ls looks stronger than the actual coupling constant because of the self resonance at nearly 3 MHz. We experimented of the receiving with the MCDR antenna at nearly 1.62 MHz and of the sending from the MCDR antenna at nearly 2.02 MHz.

We proved the communication ability of the MCDR antenna. We employed the flat sorenoidal coil as the

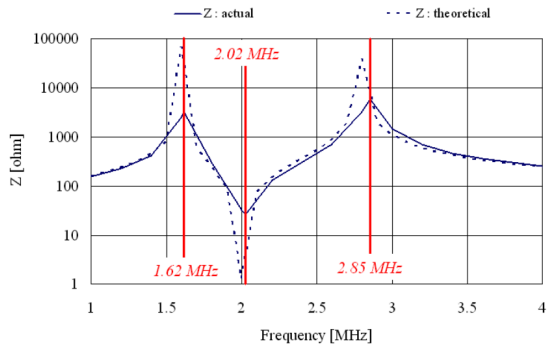

Fig. 3-6. Frequency dependence of the impedance of the MCDR antenna. Measured value is shown in full line, and theoretical value from equation (1) is shown in dash line.

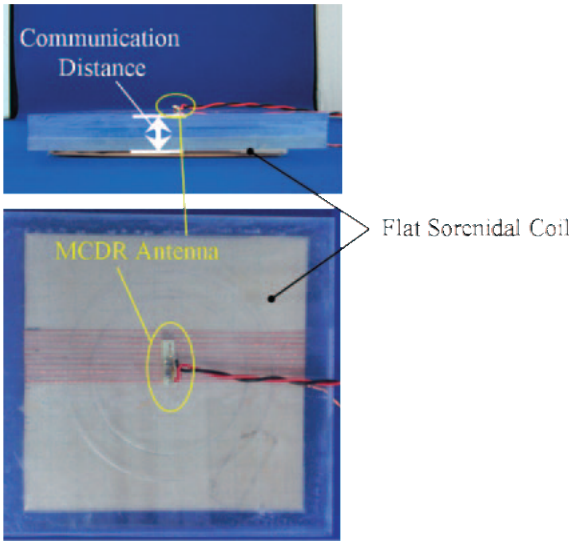

Fig. 3-7. Appearance of communication experiment. The MCDR antenna is set at the easiest communication position. Communication distance is determined as the distance between the both of coils

mounted coil shown in Fig. 3-7 [5]. The MCDR antenna was set at the location and degree at which the communication is the easiest. Although there are some problems with displacement or rotation of implanted elements, these are solved by the mounted coil and we did not evaluate them. Alternating the distance between the MCDR antenna and the flat sorenoidal coil, we sent 10000 bits and measured the Bit Error Rate (BER) at the distance. Modulation method was Phase Shift Keying (PSK), driving voltage was 3.3 V and baud rate was 115.2 kbps.

The result is shown in Fig. 3-8. In this experiment, we obtained the result that the receiving distance at the MCDR antenna was 90 mm and the sending distance from the MCDR antenna was 60 mm. In the clinical usage, implanted elements are buried under the depth of 10 – 20 mm. Therefore this result we obtained is enough to realize DFM for FES.

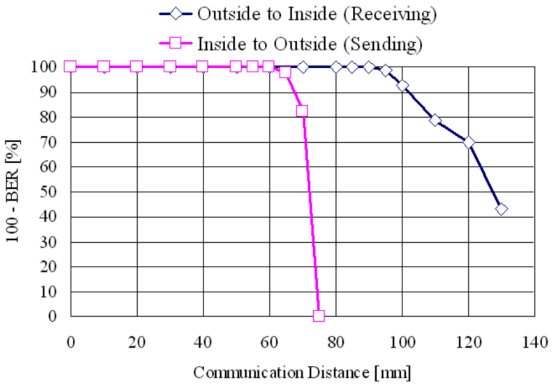

Fig. 3-8. Result of communication experiment. It shows the communication error rate to 10000 bits at the 115.2 kbps. If the value of "100 - BER" is 100 %, it means complete communication.

3.5. Summary of FES

In the DFM for FES, duplex communication function of the implanted elements is absolutely necessary for more smooth rehabilitation and safe therapy. In order to realize this function, we proposed the MCDR antenna, which has two resonant circuits connected magnetically each other. We analyzed and found that there are the best coupling coefficient for duplex communication. In addition, analyzing the impedance of the MCDR antenna, we obtained the method of design. With this design method, we made the MCDR antenna and tried communication experiment. In consequence, we verified the duplex communication ability of the MCDR antenna and succeeded the duplex communication at the distance of 60 mm. This indicates that the MCDR antenna is suitable for an implanted antenna for FES by DFM.

4. Real-time Internal Dose Measurement System

Radiation therapy is a cancer treatment that is used together with other cancer treatments, for example, surgery and chemotherapy. Radiation therapy includes two types of treatments, external beam therapy and brachytherapy. In this study, we focus on the former, in which the radiation source is located outside the body and the beam is focused onto the tumor. Recently, with advances in image diagnosis processors such as computed tomography (CT) and magnetic resonance imaging (MRI), the position and size of the tumor can be measured. Therefore, irradiation accuracy has improved, but excessive irradiation still occurs because the actual delivered dose to the tumor is unknown, so a system that measures the internal radiation dose is needed. The only radiation dose measurement system is DVS (Dose Verification System) from Sicel Technologies [5]. A radiation sensitive field effect transistor (RADFET) is used as an X-ray detector, and is 2 mm in diameter and 18 mm in length. Radiation

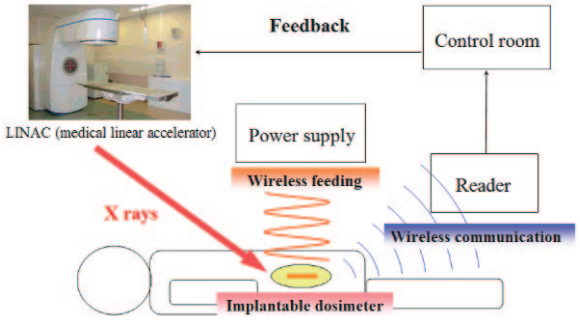

Fig. 4-1. Real-time internal radiation dose measurement system

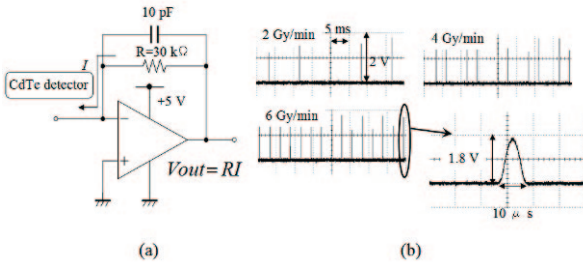

Fig. 4-2. Measurement of the output signal from the CdTe detector. (a) Current-to-voltage converter. (Equation describes the output of the converter.) (b)Current waveform at each dose rate and an expanded view of one current pulse

dose data can be transmitted only after radiation therapy, so excessive radiation cannot be prevented by DVS during the therapy. Therefore, a system for measuring the internal radiation dose in real time is required. We propose a real-time internal radiation measurement system, as shown in Fig. 4-1. This system consists of an implantable dosimeter and a wireless communication system. In this study, we report on the wireless communication system and an internal circuit to obtain radiation dose data [5,7,8].

4.1. Real-time internal radiation dose measurement system and CdTe detector

When a tumor is irradiated with X-rays by an external radiation machine, such as a medical linear accelerator (LINAC), the radiation dose is measured by an implanted dosimeter with an X-ray detector. The radiation dose data are converted into digital data and transmitted outside the body by a wireless communication system inside the body. The measurement and transmission of the internal radiation dose data are performed in real time during radiation therapy. This feedback of the transmitted data from a control room to an external irradiation machine allows exact irradiation. The wireless communication system, constructed by magnetic coupling with the structure of two coils located inside and outside the body, is unique. Considering a layer of fat, a layer of muscle, and an abdominal cavity, it should operate over a range of at least 200 mm. The dosimeter does not include a battery, so a wireless feeding system is needed to drive the dosimeter. This is also realized by a magnetic field using a feeding coil like the wireless communication system. The implantable dosimeter includes an X-ray detector, an internal coil, and a circuit. It is injected near the tumor with a syringe or a catheter.

The real-time internal radiation dose measurement system uses a cadmium telluride (CdTe) detector, which is a semiconductor detector, as an X-ray detector. When a CdTe detector is irradiated with X-rays, electrons and holes are generated and move towards electrodes due to a potential difference. The CdTe detector output charges as the radiation dose data and the signals from the CdTe detector change in proportion to the radiation dose. To confirm the output from the CdTe detector, a current-to-voltage converter circuit is used as shown in Fig. 4-2(a). The current-to-voltage converter is a circuit that performs current to voltage transformation. We measured the circuit's output when X-rays were incident on the CdTe detector from a distance of 100 cm at 2 Gy/min, 4 Gy/min, and 6 Gy/min (Gy/min is the unit of absorbed radiation dose per minute. 1 Gy means the absorption of one joule of radiation energy by one kilogram of matter.). Figure 4-2(b) shows the output of the circuit and an expanded view of one current pulse. We found that the output current waveforms were periodic pulses. Using the output voltage and circuit resistance (R), the maximum value of the current was 60 μA by the equation in Fig. 4-2(a).

4.1.1. Wireless communication system

The wireless communication system consists of two signal transmission coils, the modulation and demodulation circuits [5,7,8]. Two signal transmission coils were prepared, as shown in Fig. 4-3. The solenoid coil is used as an internal coil. It is 10mm in length and 0.7 mm on each side in cross section and consists of a ferrite core and 100-turn coil. The cross coil is used as an external coil [5]. It is also a solenoid coil that has been flattened normal to its length. It consists of a plane ferrite core of 135 mm in length, 240 mm in width, and 0.8 mm in thickness, and two 7-turn coils, one on the left side and one on the right. The direction of the coils is similar, and they are connected electrically. Each coil is displaced 40 mm from the center line.

The communication capability was examined using the internal coil, external coil, modulation circuit, and demodulation circuit, as shown in Fig. 4-3. Our modulation method was BPSK (Binary Phase Shift Keying) and the carrier frequency was 3 MHz [7]. We used the original signal data consisting of 10,000 bits of digital data prepared by a PC and sent them by the internal coil. The external coil received the signal data,

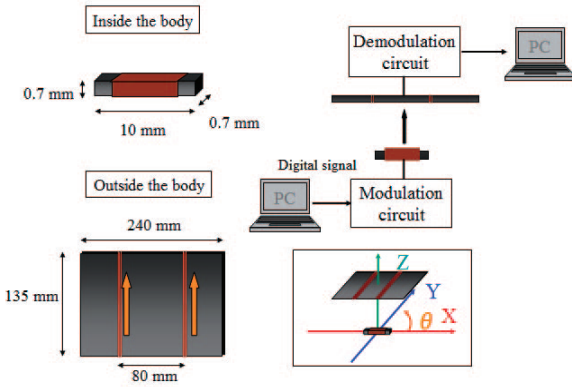

Fig. 4-3. Signal transmission coils and measurement circuit of the communication area

which was demodulated and input to the other PC. It was compared with the original signal data, and the bit error rate (BER) was measured. BER is the ratio of the number of incorrect bits transmitted to the total number of bits. We defined successful communication as the BER being zero. The transmission rate was 115.2 kbps, and the supply voltage of the modulation circuit was 2 V. The permissible relative coil-to-coil displacement and rotation were measured by moving the external coil along the X- or Y-axis and rotating the external coil.

4.1.2. Internal circuit configuration

Fig. 4-4 shows the internal circuit configuration. As shown in Fig. 4-2(b), the output from the CdTe detector is extremely minute; therefore, a signal amplification circuit should be used. The amplified signal is converted into digital data by a pulse-width modulation (PWM) circuit. Then the data are transmitted from the inside to outside of the body by the wireless communication system. The radiation dose is determined by the total charges from the CdTe detector, so we used an integrating circuit that employed an operational amplifier as a signal amplification circuit. The total charges from the CdTe detector are calculated by equation (4-1).

$$Q_{out} = CV_{out} \qquad (4\text{-}1)$$

The radiation dose is determined from Qout.

Figure 4-5(a) presents the integrating circuit. A MOSFET is used as a reset switch to discharge all stored charges in a capacitor. The maximum value of the output current from the CdTe detector is 60 μA, so we set the value of the capacitor to 1800 pF, and input square signals to the MOSFET every 30 ms as the reset signal. The output waveforms of the integrating circuit were measured when the CdTe detector was irradiated by the X-rays, at changing dose rates of 2 Gy/min, 4 Gy/min, and 6 Gy/min. As shown in Fig. 4-5(b), the output charges from the CdTe detector were stored in the capacitor at each dose rate, and all stored charges were discharged by reset pulses. However, there is a constant offset voltage of 250 mV in the output voltage at each dose rate. By removing the offset voltage outside the body, the correct output charges are calculated by equation (4-2).

$$Q_{out} = C(V_{out} - V_{offset}) \qquad (4\text{-}2)$$

A signal transmission experiment was performed to confirm whether the radiation dose data was obtained outside the body. We used the internal circuit, signal transmission coils, and the demodulation circuit. The simulated signal from the CdTe detector was input to the internal circuit, and the received signal was measured. Figure 4-6 shows the simulated signal at 6 Gy/min and the reset pulses. The frequency, pulse width, and amplitude of the signal were 350 Hz, 10 μs, and 6 V, respectively. Reset pulses were input to the MOSFET every 10 ms, and the capacitor of the integrating circuit was 650 pF. The supply voltage of the internal circuit was 2 V. The communication distance was 200 mm, and the relative displacement between the internal and external coils was zero.

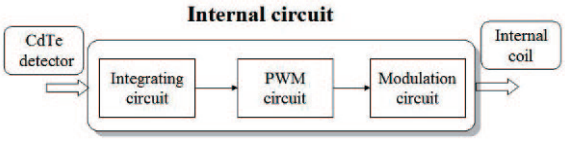

Fig. 4-4. Internal circuit configuration. Internal circuit consists of integrating, PWM, and modulation circuits.

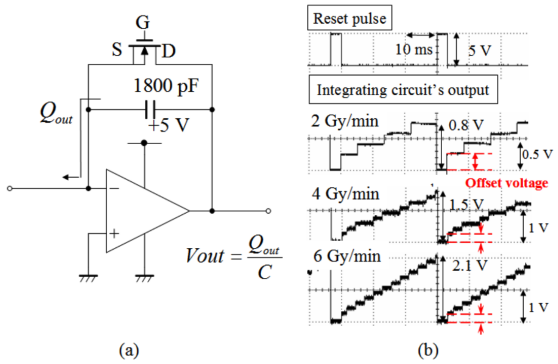

Fig. 4-5. (a) Integrating circuit. Equation describes the output of an integrating circuit. (b) Reset pulses and the output of the integrating circuit

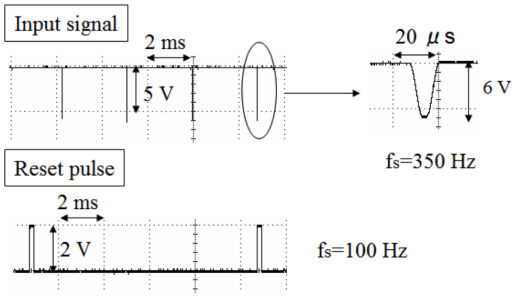

Fig. 4-6. Input signal simulating the signal from the CdTe detector

4.2. Experimental results and discussion

(i) Measurement of communication area by using wireless communication system

Figure 4-7 shows the communication coverage area. When the external coil was located at the origin, i.e., the relative displacement along the X- and Y-axis was zero, the communication distance was 300 mm along the Z-axis. When the communication distance was the required 200 mm, the permissible relative displacement was 150 mm along the X-axis and 200 mm along the Y-axis. For rotation, communication was possible at an angle of 90°. Considering symmetry along the X- and Y-axis indicates that communication was possible through any angle. When the communication is performed, the magnetic field strength emitted by the internal coil is 15 μT and the frequency of that field is 3 MHz. The interlinkage magnetic flux of the external coil is 60 nT. The communication is possible if the interlinkage magnetic flux of the external coil satisfies above the value. We confirmed that a communication distance of 200 mm could be obtained by the wireless communication system.

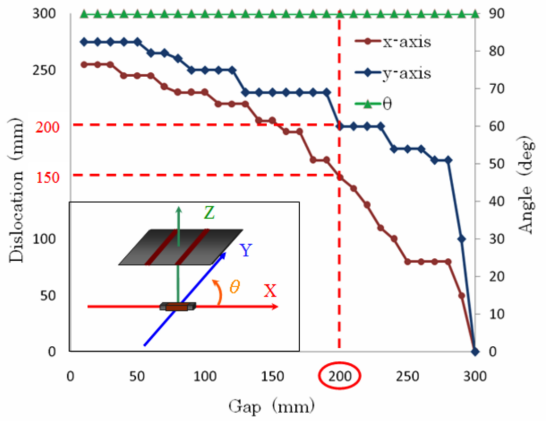

Fig. 4-7. Communication area. haracterized by relative coil-to-coil displacement and rotation.

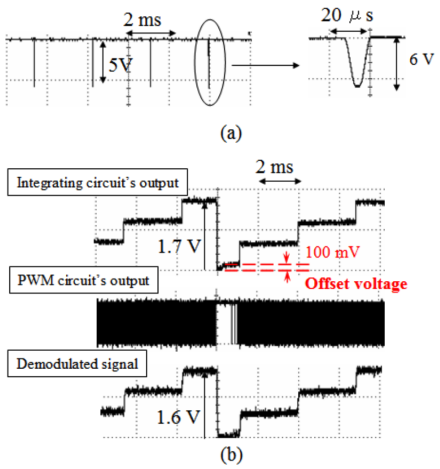

Fig. 4-8. Transmitted waveforms when the communication distance was 200 mm. Output waveforms of the internal integrating and PWM circuits, and the demodulated signals from received signals.)

(ii) Signal transmission experiment by using the internal circuit

Figure 4-8 shows the output of the integrating circuit, the output of the PWM circuit and the demodulated signal from the received signal. There was an offset voltage of 100 mV in the integrating circuit's output, so the total charges are 1014 pC by equation (4-2). The offset voltage included in the output of the integrating circuit was removed by the PWM circuit, so the total charges calculated from the demodulated signal are 1020 pC by the equation (4-1). We confirmed that radiation dose data were transmitted and demodulated without error when the communication distance was 200 mm. In conclusion, the delivered dose to the tumor is determined from the received signal using the internal circuit and the wireless communication system.

4.3. Summary of real-time internal dose measurement system

In this study, we examined a wireless communication system that communicates between the inside and the outside of the body, and an internal circuit for obtaining radiation dose data. We used a solenoid coil as an internal coil, a cross coil as an external coil, BPSK modulation, and demodulation circuits. The required communication distance was achieved. Next, an internal circuit was developed, and a signal transmission experiment was performed. The radiation dose rate is determined by the total charge output of the CdTe detector; therefore, an integrating circuit was used as a signal amplification circuit. We confirmed that radiation dose data were transmitted and demodulated without error, and the dose was determined from the received signal. In the future, a wireless feeding system to drive the internal circuit is needed. The power consumption of the internal circuit is 50 mW, therefore, a feeding coil that provides it with enough electrical power should be developed.

References

[1] Murakami K and Matsuki H. *Thermosensitivity magnetism applied engineering*. Baifu-kan, Tokyo, 48-50, Baifukan, 1993.

[2] Matsuki H. *Bioelectromagnetic Engineering*. Corona Publishing Co. LTD, Tokyo, 125-128, 1999.

[3] Rattay F. *Electrical nerve stimulation: theory, experiments and applications*. Wien, 1990.

[4] Sato F, Nomoto T, and Matsuki H. A new Contactless Power-Signal Transmission Device forImplanted Functional Electrical Stimulation. *IEEE Trans Magn* **40**, 2964-2966, 2004.

[5] Jinguuji N and Matsuki H. Transcutaneous Signal-Transmission System Using Cross Coils. *J Magn Soc Jpn* **22**, 745-748, 1998.

[6] Scarantino CW, Ruslander DM, Rini CJ, Mann GG, Nagle HT, and Black RD. An implantable radiation dosimeter for use in external beam radiation therapy. *Med Phys* **31**, 2658-2671, 2004.

[7] Takahashi M, Watanabe K, Sato F, and Matsuki H. Signal Transmission System for High Frequency Magnetic Telemetry for an Artificial Heart. *IEEE Trans Magn* **37**, 2921-2924, 2001.
[8] Somekawa T, Takura T, Sato F, Matsuki H, and Sato T. Prototype of Full-duplex Communication for Implantable Signal Transmission System of Magnetic Eight-Figure Coil. *J Magn Soc Jpn* **31**, 2007.